The frequency dependence of hygro-expansive scaling of oak

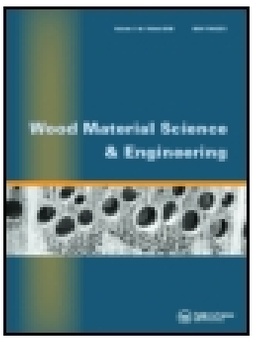

Wood Material Science & Engineering

ISSN: 1748-0272 (Print) 1748-0280 (Online) Journal homepage: http://www.tandfonline.com/loi/swoo20

The frequency dependence of hygro-expansive scaling of oak

T. Arends, L. Pel & D. M. J. Smeulders

To cite this article: T. Arends, L. Pel & D. M. J. Smeulders (2018): The frequency dependence of hygro-expansive scaling of oak, Wood Material Science & Engineering, DOI: 10.1080/17480272.2018.1472141

To link to this article: https://doi.org/10.1080/17480272.2018.1472141

Published online: 12 May 2018.

WOOD MATERIAL SCIENCE & ENGINEERING
https://doi.org/10.1080/17480272.2018.1472141

Taylor & Francis
Taylor & Francis Group

The frequency dependence of hygro-expansive scaling of oak

T. Arends[a], L. Pel[a] and D. M. J. Smeulders[b]

[a]Department of Applied Physics, Eindhoven University of Technology, Eindhoven, Netherlands; [b]Department of Mechanical Engineering, Eindhoven University of Technology, Eindhoven, Netherlands

ABSTRACT

Fluctuations in the ambient relative humidity are often cyclic of nature, composed of a wide variety of frequencies. Variations may be as fast as one minute or as slow as a complete season. A wooden object exposed to these fluctuations exchanges moisture with the air, resulting in a change in the local moisture content of the wood. Since moisture penetration is affected by the timescale of the changes in ambient conditions, so are processes caused by moisture content variations. Moisture content variations cause dimensional changes of a wooden object, which, if mechanically restrained, lead to a buildup of stresses and ultimately to damage. It is therefore important to predict the frequency behavior of moisture content and expansion in wood. In the presented study, experiments are conducted in which the moisture content and expansion of oak cubes with different sizes is measured during sinusoidal relative humidity fluctuations with different frequencies. The amplitude in moisture content and expansion is shown to be simply scalable based on sample size only. Derived diffusion coefficients are in agreement with literature values, although the experimental frequency behavior is shown to deviate qualitatively from diffusive frequency behavior.

ARTICLE HISTORY
Received 20 September 2017
Revised 5 March 2018
Accepted 30 April 2018

KEYWORDS
Moisture transport; deformation; frequency behavior; experimental study; non-destructive evaluation on wood and wood-based materials

Introduction

Examples of wood objects exposed to a fluctuating environment are abundant, e.g. furniture, parquet floors, structural elements, or art objects. During these dynamically changing conditions, the moisture in the material is not in equilibrium with the moisture in the surrounding air. As a consequence, moisture transport takes place from or toward the exposed surface, resulting in a continuously changing local moisture content. In wood, a change in the moisture content is associated with dimensional changes; an increase in the moisture content results in expansion, a decrease causes shrinkage (Skaar 1988). As a result, stresses develop in the material if free expansion is obstructed. These stresses can rise as high as the yield stress or even the strength of the material (Mecklenburg and Tumosa 1996), resulting in damage. This is undesirable; knowledge about deformation during dynamically changing relative humidity conditions is therefore important.

Moisture transport in wood and its implications on deformation have been extensively studied both numerically and experimentally (Dahlblom *et al*. 1996, Ormarsson *et al*. 1998, Svensson and Toratti 2002, Jakiela *et al*. 2008, Gamstedt *et al*. 2013, Larsen and Ormarsson 2013, Mazzanti *et al*. 2014, Joffre *et al*. 2016). Many experimental studies on hygroscopic expansion of wood consider only stepwise changes in the relative humidity (Zhou *et al*. 1999, Murata and Masuda 2006, Senni *et al*. 2010, Caré *et al*. 2012, Derome *et al*. 2012, Gauvin *et al*. 2014). This condition is, however, rare in real-life applications, except in extreme cases, e.g. during flooding or air-conditioning failure (van Schijndel *et al*. 2010). Changes of environmental conditions are usually continuous, often manifested in daily or seasonally repeating cycles (Forest Products Laboratory 2010). An example is shown in Figure 1(a), where the time evolution of the relative humidity over the course of 3 years is shown outside the St. Bavo Cathedral in Ghent, Belgium (http://www.monumenten.bwk.tue.nl/CfC). The frequency spectrum after discrete Fourier transform, shown in Figure 1(b), clearly demonstrates peaks at dominant fluctuation frequencies, with periods of one day and one year.

Knowing the hygromorphic response of wood under these cyclically changing relative humidity conditions has therefore a practical relevance. Some examples exist of studies where cyclic relative humidity fluctuations are considered in wood hygromechanics, e.g. with triangular relative humidity fluctuations (Ma *et al*. 2005), or sinusoidal fluctuations (Chomcharn and Skaar 1983, Schellen 2002, Yang and Ma 2014). In these studies, the response in only a narrow range in fluctuation frequencies is studied, with periods of 5.66 hours up to 27 hours. Objects may, however, also be exposed to higher frequencies in relative humidity changes; groups of visitors with wet clothes passing a wooden art object exhibited in a museum every several minutes can be considered a high-frequency relative humidity fluctuation. The size of the object also plays a role; the relative moisture penetration at a certain high frequency will be larger in a small or thin object compared to a large or thick object. The expansive response will therefore be dependent on the object geometry and the frequency of the fluctuations. In other words, there might be some sort of scaling in the frequency response of wood objects, based on the size of the object and the frequency of the fluctuation.

CONTACT L. Pel l.pel@tue.nl

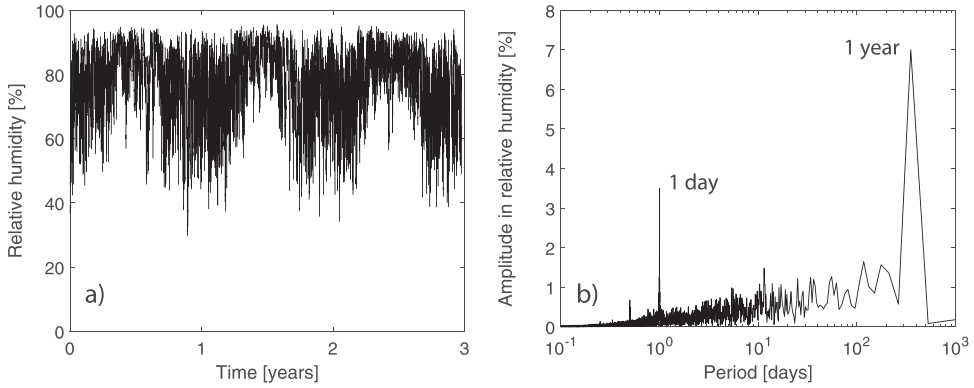

Figure 1. (a) The time evolution of the relative humidity outside the St. Bavo Cathedral in Ghent, Belgium, over the course of three years. (b) The frequency spectrum after Fourier transform, clearly showing several peaks at dominant fluctuations frequencies.

In this study, we examine the frequency dependence of the expansion of differently sized oak cubes exposed to sinusoidally varying relative humidity. The goal is to find the size scaling in the frequency behavior using a simple model. To this end, experiments and numerical calculations are performed. A theoretical background for the scaling based on the diffusion equation and the assumption of the sample as a linear system is presented first, after which the experimental set-up and numerical simulations are described. Experimental and numerical results are shown and discussed, and compared to the theory. Finally, conclusions are drawn and an outlook is presented.

Theory

In this study, we are interested in moisture transport and consequent expansion of cubic oak samples. Moisture transport in a porous medium is often described by a diffusion equation. Although it may not always concern a pure diffusion process, the driving forces can be rewritten to arrive at the form of Fick's second law, which will be the starting point of the theory presented here. Since no analytical solutions exist describing three-dimensional diffusion in a rectangular geometry, diffusion in a sphere will be analyzed first. Let us consider an isotropic sphere with radius R, exposed to a step change in the moisture content at its surface. This problem can be formulated mathematically as

$$\begin{cases} r^2\partial_t c = D\partial_r(r^2\partial_r c), \\ c(r,0) = c_0, \\ \partial_r c(0,t) = 0, \\ c(R,t) = c_s, \end{cases} \tag{1}$$

where r is the radial coordinate, c the moisture content, D the constant diffusion coefficient, c_0 the initial moisture content, and c_s the moisture content imposed at the boundary. An analytical solution can be obtained by separation of variables (see, e.g. Strauss (2008) or Crank (1975)). The result can be formulated in the form of the Fourier series:

$$c(r,t) = c_s - 2R\frac{c_s - c_0}{\pi r}\sum_{n=1}^{\infty}\frac{1}{n}\sin\left(\frac{n\pi r}{R}\right)e^{-D(n\pi/R)^2 t}. \tag{2}$$

Equation (2) already elucidates two scaling parameters: a dimensionless position along the radius (r/R), and a typical diffusion time (R^2/D). Since the moisture content of a sample as a whole is measured during experiments, rather than the local moisture content, Equation (2) can be integrated to obtain the evolution of the total moisture content (Crank 1975). The normalized moisture content of the sphere m_s^* can then be expressed as

$$m_s^*(t) = \frac{m - m_0}{m_\infty - m_0} = 1 - \frac{6}{\pi^2}\sum_{n=1}^{\infty}\frac{1}{n^2}e^{-D(n\pi/R)^2 t}. \tag{3}$$

We can now substitute the scaled time $t_R^* = Dt/R^2$ in Equation (3) to arrive at

$$m_s^*(t_R^*) = \frac{m - m_0}{m_\infty - m_0} = 1 - \frac{6}{\pi^2}\sum_{n=1}^{\infty}\frac{1}{n^2}e^{-(n\pi)^2 t_R^*}. \tag{4}$$

So far the material was assumed to be isotropic, i.e. with moisture transport independent of the direction. In wood, however, moisture transport along the longitudinal direction occurs much faster, with coefficients at least an order of magnitude larger (Siau 1984). We can therefore approximate the moisture transport process as one-dimensional along the predominant longitudinal direction, thereby omitting the contribution of the radial and tangential direction on the overall moisture transport. The moisture content evolution is then similar to a slab with thickness d, exposed to moisture on two opposite sides as (Crank 1975):

$$m_C^*(t^*) = 1 - \frac{8}{\pi^2}\sum_{n=0}^{\infty}\frac{1}{(2n+1)^2}e^{-(2n+1)^2\pi^2 t^*}, \tag{5}$$

with $t^* = Dt/d^2$. To relate the approximation of the cube as a sphere and as a slab, a conversion between the radius R of a sphere and the thickness d of a cube can be introduced based on equality in volume. This yields $d = aR$, with $a = \sqrt[3]{4\pi/3}$, which will be used in the following to convert t_R^* to t^*.

The sums in Equations (4) and (5) quickly converge (Talbot and Kitchener 1956), and hence the moisture content can be approximated by taking into account only the first few modes. The moisture content evolution in both Equations (4) and (5)

can be approximated by

$$m_{\mathrm{A}}^{*}(t^{*}) = 1 - e^{-\gamma\pi^{2}t^{*}}, \tag{6}$$

with $\gamma = a^2$ or 1 for the approximation of the cube as a sphere and as a slab respectively. Equations (4)–(6) are plotted in Figure 2(a) as a function of the square root of t^*. Discrepancies at short times t^* are seen; the initial increase in moisture content of Equations (4) or (5) is linear, whereas this region is non-linear for Equation (6).

Since natural relative humidity fluctuations are often cyclic, composed of different frequencies, we are interested in the frequency behavior of the moisture content. Assuming that the moisture content evolution of the cube behaves as a linear system, we can acquire the frequency behavior by first determining the transfer function of the systems represented by Equations (4)–(6). The transfer function $H(s)$ in terms of the complex variable s relates the input function and the response of a linear system in the Laplace space (Franklin *et al*. 1994) as

$$X(s) = H(s)U(s), \tag{7}$$

where X and U are the Laplace transforms of the output and input function respectively. For diffusion in a sphere, X is the Laplace transform of Equation (3):

$$X_{\mathrm{S}}(s) = \mathcal{L}\{m_{\mathrm{S}}^{*}(t)\} = \frac{1}{s} - \frac{6}{\pi^{2}}\sum_{n=1}^{\infty}\frac{1}{n^{2}}\frac{1}{D\left(\frac{n\pi}{R}\right)^{2} + s}. \tag{8}$$

Equation (4) is the time response to a step change in the scaled moisture content at the boundaries from 0 to 1. Note that this is the step in equilibrium moisture content which the sample eventually reaches. The transfer function $H(s)$ of the system is derived with the Laplace transform of the input function

$$U(s) = \mathcal{L}\{u(t)\} = \frac{1}{s}, \tag{9}$$

and with Equations (7) and (8) to arrive at

$$H_{\mathrm{S}}(s) = 1 - \frac{6}{\pi^{2}}\sum_{n=1}^{\infty}\frac{1}{n^{2}}\frac{s}{D\left(\frac{n\pi}{R}\right)^{2} + s}. \tag{10}$$

To analyze the frequency behavior, we consider $H_{\mathrm{S}}(i\omega)$, with ω the angular frequency:

$$H_{\mathrm{S}}(i\omega) = 1 - \frac{6}{\pi^{2}}\sum_{n=1}^{\infty}\frac{1}{n^{2}}\frac{i\omega D\left(\frac{n\pi}{R}\right)^{2} + \omega^{2}}{D^{2}\left(\frac{n\pi}{R}\right)^{4} + \omega^{2}}. \tag{11}$$

At this point, we can relate two timescales: the transport timescale (d^2/D) to the relative humidity fluctuation timescale (f^{-1}). The ratio of the two timescales is a measure of the relative penetration of externally applied fluctuations, and is introduced as the dimensionless frequency f^*:

$$f^{*} = \frac{fd^{2}}{D} = a^{2}\frac{fR^{2}}{D}, \tag{12}$$

where f is the ordinary frequency in Hertz. We can use this dimensionless frequency and use $f = \omega/2\pi$ to rewrite the transfer function corresponding to the approximation of the cube as a sphere (Equation (11)) to arrive at

$$H_{\mathrm{S}}(if^{*}) = 1 - \frac{6}{\pi^{2}}\sum_{n=1}^{\infty}\frac{1}{n^{2}}\frac{i\frac{2f^{*}}{\pi a^{2}n^{2}} + \left(\frac{2f^{*}}{\pi a^{2}n^{2}}\right)^{2}}{1 + \left(\frac{2f^{*}}{\pi a^{2}n^{2}}\right)^{2}}. \tag{13}$$

Similarly, we can determine the transfer function corresponding to the one-dimensional approximation of the cube as a slab (Equation (5)) as

$$H_{\mathrm{C}}(if^{*}) = 1 - \frac{8}{\pi^{2}}\sum_{n=0}^{\infty}\frac{1}{(2n+1)^{2}}\frac{i\frac{2f^{*}}{\pi(2n+1)^{2}} + \left(\frac{2f^{*}}{\pi(2n+1)^{2}}\right)^{2}}{1 + \left(\frac{2f^{*}}{\pi(2n+1)^{2}}\right)^{2}}. \tag{14}$$

The amplitude as a function of the frequency f^* can be determined as the absolute value of the transfer function, i.e. its modulus. No concise expression can be found for the moduli of Equations (13) and (14). For the first-order approximation, i.e. the single exponential in Equation (6), a simple expression for the scaled amplitude A_{S}^{*} as a function of dimensionless frequency can be formulated as

$$A_{\mathrm{S}}^{*}(f^{*}) = \frac{1}{\sqrt{1 + \left(\frac{2f^{*}}{\gamma\pi}\right)^{2}}}. \tag{15}$$

The moisture content amplitude as a function of frequency of different sample sizes and diffusion coefficients can thus be scaled with the dimensionless frequency using Equation (12). A familiar way to visualize amplitude–frequency relations in the field of dynamic systems is by means of a Bode amplitude plot (Franklin *et al*. 1994). Equation (15) and the moduli of Equations (13)–(14) are shown in Figure 2(b) as a function of f^*. Three dimensionless frequency regions can be distinguished. For low f^*, i.e. for fluctuations much slower than internal moisture transport, the amplitude reaches a constant value since the sample is in equilibrium at all times. For $f^* \approx 1$, an inflection in the amplitude is observed toward lower values, due to the same timescale of the imposed changes and the transport in the material. In the final region, for high values of f^*, the changes are faster than transport and a decline in amplitude is seen with a constant slope on a logarithmic scale. The slope of the approximation of the cube as a sphere and as a cube has a value of −0.5; the modulus of Equation (15) has a slope of −1 at high dimensionless frequencies. This is a result of the omission of higher modes, which have an influence at short times t^*, and hence at high dimensionless frequencies f^*.

In wood, a change in the moisture content is associated with a change in dimension. The simplest way to relate moisture content changes in the sample to expansion is to assume a cross-section does not deform. Although the deformation of wood due to local moisture-induced expansion is more complex than presented and governed by multiple mechanical properties, here the expansion ε is assumed to follow

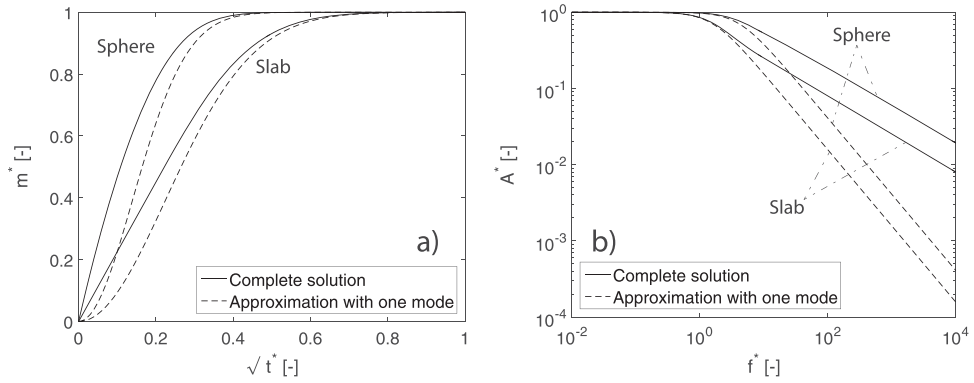

Figure 2. (a) Normalized moisture content as a function of the scaled time t^* in a cube approximated as a sphere (3D transport) or as a cube (1D transport), following a step change in the moisture content at the boundaries. (b) Amplitude in normalized moisture content as a function of the dimensionless frequency f^*.

the simple relation:

$$\varepsilon = \alpha \int_0^d c\,dx, \tag{16}$$

where α is the linear hygroscopic expansion coefficient. The expansion is directly related to the change in integrated moisture content. In other words, the expansion can be scaled to arrive at the same time evolution as (e.g. Equations (4)–(6)):

$$\varepsilon^* = \frac{\varepsilon}{\alpha \Delta c} = m^*. \tag{17}$$

The expansion has the same time evolution as the moisture content; hence, it is assumed to have the same frequency behavior. As a consequence, the scaling as derived above is applicable to the expansive frequency behavior too.

Materials and methods

Oak cubes with different dimensions (sides of 2, 4, 6, 8, and 10 mm) were prepared from a large board. The samples with sides of 2 mm contained only one annual ring and a few vessels; hence, their microstructure is poorly representative. The larger samples contained multiple annual rings and vessels and are more representative for oak. In each experiment, two equally sized cubes were exposed to the same condition. One of the samples was used to determine the moisture content gravimetrically; the other sample was used to measure the one-dimensional expansion. To this end, an experimental set-up was constructed which consists of a thermogravimetric analyzer, a thermomechanical analyzer. In the humidifier, a dry and a wet air stream are mixed to generate an air flow with adjustable relative humidity (Arends *et al.* 2017). The air flow leaving the humidifier is then divided over two parallel circuits. One sample was placed on the balance of a Mettler Toledo TG50; the mass of the sample was measured while exposed to the air stream. The other part of the air flow leaving the humidifier was blown over a sample placed under a probe of fused silica, which is part of a Mettler Toledo TMA/SDTA 841e system; local one-dimensional deformation was measured accordingly using a linear variable differential transformer with an accuracy of ~10 nm. The probe was placed in the middle of the top surface of the sample. In all experiments, the cubes were oriented such that expansion in the tangential direction was measured. The oven-dry mass and thickness of each cube were measured after the experiment to transform mass and thickness during the experiment to moisture content and expansion.

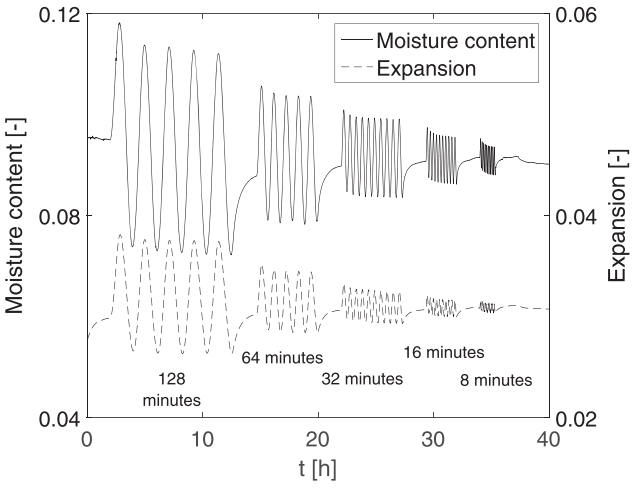

Figure 3. An example of the moisture content and expansion of two equally sized cubes over time during exposure to sinusoidal variations in relative humidity. (50 ± 40%) at different frequencies, with equilibration time between two consequent frequencies. The periods of the fluctuations are indicated in the figure.

Results and discussion

From time-domain to frequency-domain

An example of the evolution of moisture content and one-dimensional expansion of two different, equally sized samples with sides of 6 mm during exposure to sinusoidal fluctuations in relative humidity is shown in Figure 3. As can be seen, both moisture content and expansion fluctuate sinusoidally following the imposed relative humidity changes of the ambient air. Furthermore, the amplitude of the response, both in moisture content and expansion, is seen to decrease with increasing frequency. The moisture content and expansion over time can be fitted with a sine function to acquire the amplitude of the response. This is done for a wide

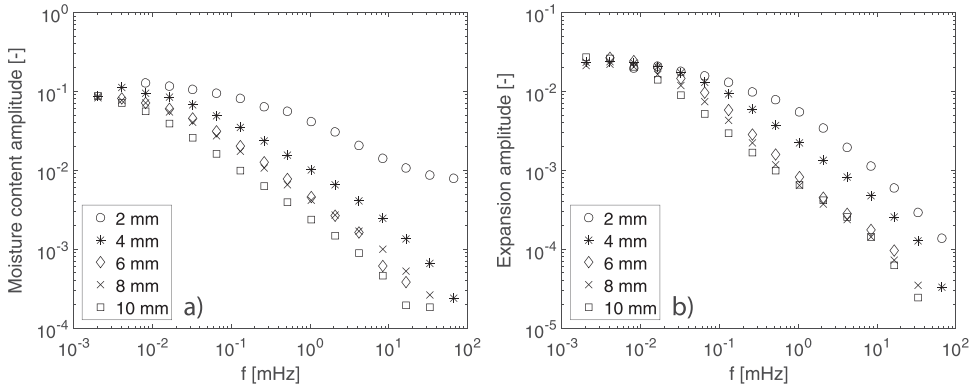

Figure 4. (a) Measured moisture content amplitude and (b) measured expansion amplitude as a function of relative humidity fluctuation frequency of oak cubes with different sizes. The lowest frequency corresponds to a fluctuation with a period of 134 hours, the highest to a period of 15 seconds.

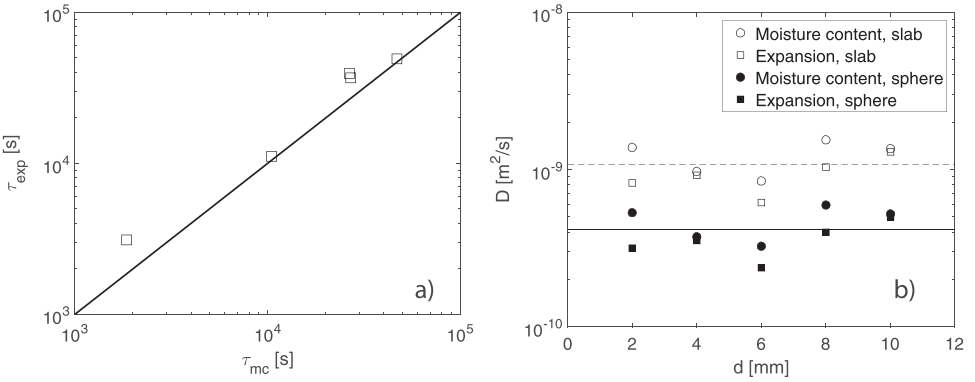

Figure 5. (a) The characteristic expansion time as a function of the characteristic moisture content time. (b) The diffusion coefficients as derived from the characteristic times for different sample sizes, for moisture transport occurring along one dominant direction (approximation as a slab) or for isotropic moisture transport (approximation as a sphere), with average values indicated by horizontal lines.

range of frequencies (periods of 132 hours to 15 seconds) of the relative humidity variation 50 ± 40%, to obtain the amplitude in moisture content and expansion as a function of frequency. The results can be visualized in Bode amplitude plots for moisture content (Figure 4(a)) and expansion (Figure 4(b)) for different sample sizes. In both plots, three regions can be distinguished, as already predicted in Figure 2(b). At low frequencies, the amplitude in moisture content and expansion reaches an almost constant value. At high frequencies, the amplitude declines with a slope almost equal for all sample sizes.

A deviation is seen in the moisture content amplitude of the 2 mm sample, with a lower slope in the high-frequency regime compared to the other samples. A probable cause for the discrepancy is the visually observable presence of two large vessels along the longitudinal direction of the sample. These more permeable regions enhance moisture transport in this small sample, reflected in a large amplitude in moisture content.

Scaling

The amplitude as a function of the frequency of the different sample sizes in Figure 4 can be fitted with the amplitude of the single exponential approximation (Equation (15) multiplied with a constant), to determine the time constant $\tau = d^2/\gamma\pi^2 D$ in Equation (6). This is done for both the moisture content and expansion amplitudes. The resulting characteristic times τ_{mc} and τ_{exp}, for the moisture content and expansion respectively, are shown in Figure 5(a). The straight line indicates equal values for τ_{mc} and τ_{exp}. As can be seen, a one-on-one correlation is found, i.e. expansion follows moisture content immediately. Values for the diffusion coefficient D, calculated from τ, are shown in Figure 5(b). Two values are shown for each sample; one assuming the sample to be isotropic in moisture transport (approximation as a sphere) and one assuming moisture transport is predominant in one direction (approximation as a slab). Average diffusion coefficients are indicated by horizontal lines, with values of 4.2×10^{-10} m^2/s and 1.1×10^{-9} m^2/s for the isotropic and anisotropic case, respectively. The first value is in good agreement with an average diffusion coefficient over the total moisture content range and the three directions reported by Saft and Kaliske (2013) for oak (3.5×10^{-10} m^2/s). Furthermore, the average diffusion coefficient over the total moisture content range for the longitudinal direction (9.5×10^{-10} m^2/s) corresponds well to the value found in this study for diffusion along one dominant direction. Moreover, it is in reasonable agreement with the diffusion coefficient obtained directly by NMR (Arends *et al.* 2018).

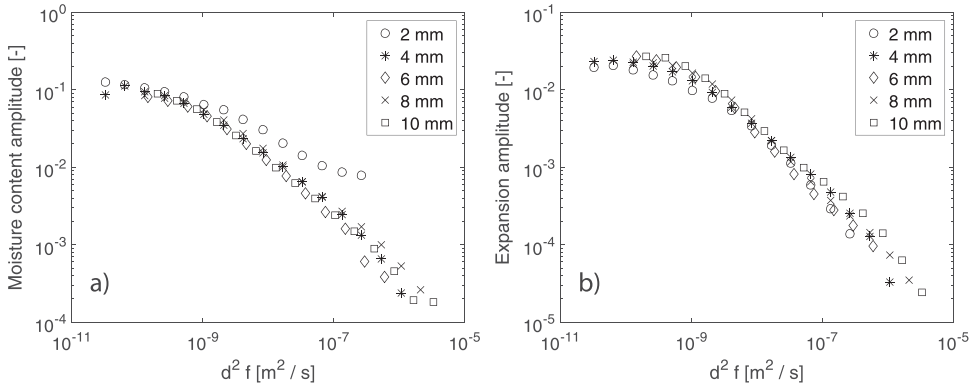

Figure 6. (a) Moisture content amplitude and (b) expansion amplitude as a function of the frequency multiplied by the sample thickness squared.

The results shown in Figure 4 can, according to theory, be scaled by multiplication of the frequency with d^2 for the different sample sizes (see Equation (12)). The result is shown in Figure 6(a,b) for the amplitude in moisture content and expansion, respectively. As can be seen, this results in one master curve for the different sample sizes for over three orders of magnitude in amplitude. A size effect, as reported in previous studies on moisture sorption in wood (Wadsö 1994a, Krabbenhoft and Damkilde 2004), would result in the amplitudes of the different samples to be distinguishable even after scaling. Such an effect is absent here; effective scaling can be obtained based only on the sample size.

The Bode plots in Figure 4 can be scaled with the dimensionless frequency f^* introduced in Equation (12), using the calculated diffusion coefficients for the approximation of the cube as a slab in Figure 5(b). This results in dimensionless Bode plots for both the moisture content and expansion, shown in Figure 7(a,b), respectively. The scaling derived from the simple theory results in one master curve for all experimental points of the different sample sizes similar to Figure 6, both for moisture content and expansion. The diffusion coefficients in Figure 5(b) are similar for the different sample sizes; hence, Figures 5 and 6 are qualitatively similar. The insets in Figure 7 show the amplitude for high dimensionless frequencies, accompanied by a linear fit on the log–log scale. The slope of the fit is −0.78 for the amplitude in moisture content and −0.79 for the amplitude in expansion. This is steeper than the theoretical prediction resulting from the approximation of the cube as a sphere or slab (−0.5). The amplitude in moisture content and expansion thus declines faster than predicted from the diffusion equation alone.

Relating moisture content to expansion

The frequency behavior of the moisture content and the expansion of the cubes were seen to be qualitatively similar in Figure 7. This is even more apparent if the amplitude in expansion is plotted as a function of the amplitude in moisture content for the different sample sizes and different frequencies, as shown in Figure 8(a). The hygroscopic expansion coefficient is determined by a linear fit on the log–log scale as 0.35. This is in good agreement with values reported in literature for expansion in tangential direction (Forest Products Laboratory 2010, Saft and Kaliske 2013). Figure 8(a) illustrates the one-on-one relation between moisture content and expansion, as was already assumed in Equation (16). Although expansion is measured locally (in the middle of the top surface of the cube) and moisture content globally (averaged over the total sample), the simple relation between moisture content and expansion amplitude holds.

The amplitudes in both moisture content and expansion can be plotted together by dividing the amplitude in expansion by the hygroscopic expansion coefficient, as shown in Figure 8(b). The amplitudes are additionally scaled by the amplitude in moisture content at low frequencies (0.09). Again three regions can be distinguished, depending on the relation between the frequency of the changes and the capability of the sample to equilibrate. The frequency behavior resulting from the approximation of the cube as a slab (Equation (14)), and the approximation by a single exponential are also shown in Figure 8(b). In the experiments, a different quantitative frequency behavior is found when compared to diffusive frequency behavior. Only the 2 mm sample, which deviates qualitatively from the other samples, shows the same behavior, with similar slope for high f^*. The deviation of this sample was already attributed to the presence of vessels which comprise a relatively large portion of the exposed radial–tangential surface; hence, this sample is not representative.

3D numerical simulations

So far, the oak cubes have been approximated as isotropic spheres or slabs. To determine the effect of a three-dimensional rectangular geometry on the frequency behavior, numerical simulations in COMSOL© are performed. A cube, supported on its bottom surface, is exposed to a prescribed moisture content at the boundaries, varying sinusoidally. Moisture transport is described with the diffusion equation, and the material is assumed to be linear elastic. First some computations are performed assuming the material to be isotropic for both moisture transport and mechanics. Two different values for the isotropic diffusion coefficient are tested ($D_{low} = 5 \times 10^{-11}$ m^2/s, $D_{high} = 5 \times 10^{-10}$ m^2/s). Subsequently, the diffusion coefficient is presumed dominant in the

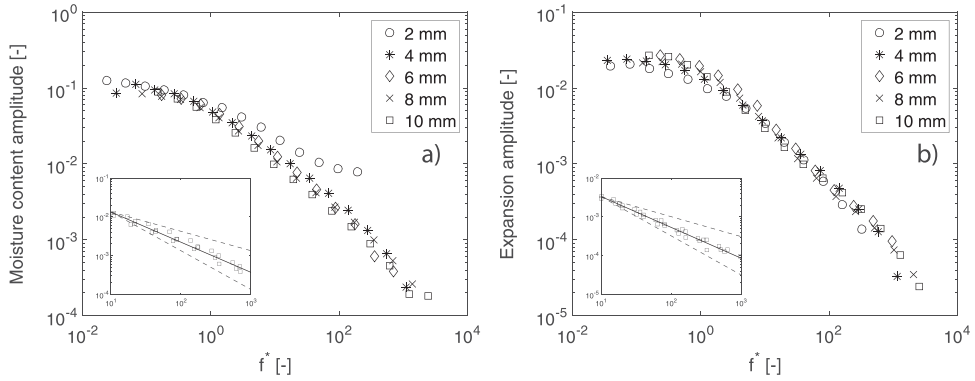

Figure 7. (a) Moisture content amplitude and (b) expansion amplitude as a function of the dimensionless frequency *f**. Insets show the amplitude for high dimensionless frequencies with linear fit on the log–log scale (solid line), and slopes of −0.5 and −1 (dotted lines).

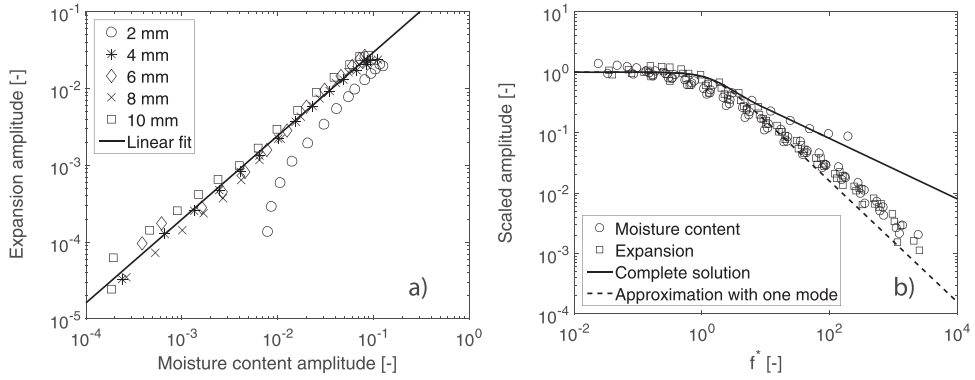

Figure 8. (a) The amplitude in moisture content versus the amplitude in expansion for the different samples and frequencies with a linear fit to retrieve the expansion coefficient (0.35). (b) Amplitude as a function of dimensionless frequency for moisture content and. expansion, where the expansion amplitude is scaled by the retrieved expansion coefficient of 0.35. The complete solution of the diffusion equation and the approximation with one mode are shown in the figure too.

longitudinal direction, but all mechanical parameters are kept isotropic. Finally, simulations are performed with values for both the diffusion coefficients and mechanical parameters dependent on moisture content and the principal direction, adapted from Saft and Kaliske (2013). In accordance with the experiments, the simulations are performed with a relative humidity fluctuation of 50 ± 40%. A non-linear sorption isotherm is assumed, with values from the Wood Handbook (Forest Products Laboratory 2010). This results in an amplitude in moisture content of ∼0.09 at the boundaries. The expansion coefficients α in the simulations are assumed to be 0.35, 0.19, and 0.016 in the tangential, radial, and longitudinal direction, respectively (Saft and Kaliske 2013). For the stiffness, an arbitrary value can be chosen if independent of the moisture content; the value for the E-modulus does not affect the results. For the Poisson-ratio υ, a value of 0.3 is assumed.

Results of the three-dimensional numerical simulations in COMSOL are shown in a dimensionless Bode plot in Figure 9(a,b) for the moisture content and expansion, respectively. The moisture content amplitude is scaled by the imposed amplitude in moisture content at the surface (0.09) and the expansion amplitude by the product of the amplitude in moisture content and the expansion coefficient in tangential direction (0.032). For simulations with a diffusion coefficient dependent on the principal direction (termed "Anisotropic" in Figure 9), an average diffusion coefficient of the three is used to calculate *f**. For moisture content dependent values of the diffusion coefficient, an average over the moisture content range is calculated for *f**. The amplitude as a function of *f** for a sphere, i.e. the modulus of Equation (13), is also shown in Figure 9.

The results of numerical simulations with cubes, with constant transport and mechanical properties or with moisture-dependent values, can be scaled onto the analytical solution for diffusion in a sphere, based on sample size and average diffusion coefficient. Furthermore, the expansive frequency behavior can be scaled equally; expansion thus follows moisture content immediately. This was also observed in experiments. Wood anisotropy can hence not explain the difference in frequency behavior as predicted from the diffusion equation and observed in experiments (Figure 8(b)). Moreover, the starting point of diffusion in a sphere, from which analytical solutions can be obtained for the frequency behavior, is seen to be justified.

Alternative moisture transport model

The experimental frequency behavior deviates from the predicted behavior of the diffusion equation. The slope for high dimensionless frequencies is larger than predictions from the diffusion equation; an additional effect attenuates the amplitude at high frequencies. Failure of the diffusion

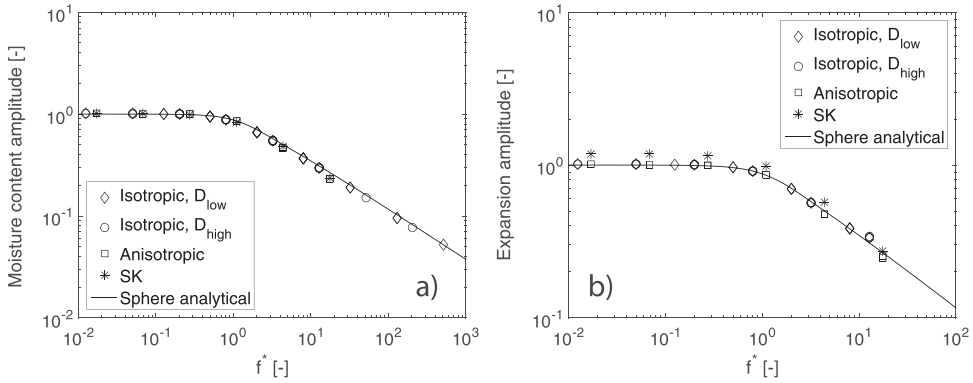

Figure 9. (a) Moisture content amplitude and (b) expansion amplitude as a function of the scaled frequency f^*, for isotropic moisture transport ($D_{low} = 5 \times 10^{-11}$ m^2/s, $d_{high} = 5 \times 10^{-10}$ m^2/s), anisotropic moisture transport ($D_{longitudinal} = 1 \times 10^{-9}$ m^2/s, $d_{radial} = d_{tangential} = 5 \times 10^{-11}$. m^2/s) with constant, isotropic mechanical properties ($\alpha = 0.35$, $E = 3$ GPa, $\upsilon = 0.3$), and the anisotropic model with moisture-dependent transport and mechanical properties proposed by. Saft and Kaliske (SK). The frequency behavior for a sphere resulting from Equation (13) is also shown. The fewer points in the expansion amplitude plot are due to the requirement of a too fine mesh to accurately describe the expansion.

equation for wood was already postulated by Wadsö (1994a) before; several models have been proposed since to account for non-Fickian effects such as step magnitude and sample size dependence of experimental results (Wadsö 1994b, Cunningham 1995, Krabbenhoft and Damkilde 2004, Dvinskikh *et al*. 2011, Eitelberger *et al*. 2011). Here numerical experiments are performed with a model proposed by Cunningham (1995) first and extended by Krabbenhoft and Damkilde (2004). In this model, the moisture in the wood is assumed to be present as water vapor in the cell cavities and as cell wall moisture. Cunningham assumed moisture transport to occur solely as vapor diffusion; sorption to the cell wall results in a change in the cell wall moisture content. Krabbenhoft and Damkilde extended the model by incorporating cell wall moisture diffusion. Mathematically, this can be formulated as

$$\begin{aligned} \partial_t w &= D_w \partial_{xx} w + h(lv - kw), \\ \partial_t v &= D_v \partial_{xx} v + h(kw - lv), \end{aligned} \tag{18}$$

where w is the moisture content in the cell wall, v the vapor concentration, D_w and D_v the diffusion coefficients for moisture transport in the cell wall and cell cavities, respectively, h the mass transfer coefficient, and k and l coefficients connecting the cell wall moisture content and vapor concentration to a driving potential for moisture sorption. It is assumed here that the ratio l/k is the slope of the sorption curve relating cell wall moisture content to vapor content, and that the water vapor and cell wall moisture are initially and finally in equilibrium. This yields $w_0 = l/k\ v_0$ and $w_{\boxed{?}} = l/k\ v_{\boxed{?}}$, with the subscripts 0 and ∞ indicating initial and final values, respectively. The equations in (18) can be made dimensionless by introducing the scaling variables

$$\begin{aligned} &v^* = l\frac{v - v_0}{v_\infty - v_0},\ w^* = k\frac{w - w_0}{w_\infty - w_0},\ D^* = \frac{D_w}{D_v}, \\ &h^* = \frac{lhd^2}{D},\ k^* = \frac{k}{l},\ t^* = \frac{D_v t}{d^2},\ x^* = \frac{x}{d}, \end{aligned} \tag{19}$$

resulting in

$$\begin{aligned} \partial_{t^*} w^* &= D^* \partial_{xx^*} w^* + k^* h^* (v^* - w^*), \\ \partial_{t^*} v^* &= \partial_{xx^*} v^* + h^* (w^* - v^*). \end{aligned} \tag{20}$$

Boundary conditions can be introduced as

$$\begin{aligned} v^*|_{x^*=0,1} &= v_S^*, \\ \partial_t w^*|_{x^*=0,1} &= k^* h^* (v_S^* - w^*). \end{aligned} \tag{21}$$

The quantity of interest is the moisture content over the sample as a whole. Since cell wall moisture accounts exclusively for expansion, the dimensionless cell wall moisture content w^* is integrated to obtain m^*. The model equations are discretized and solved in Matlab for different exposure conditions. In the simulations, first a step change in the vapor concentration at the exposed surface v_S^* from 0 to 1 is considered. Next, the frequency behavior is examined by imposing a sinusoidal fluctuation in v_S^*:

$$v_S^* = \sin\left(\frac{2\pi t^*}{f^*}\right), \tag{22}$$

with $f^* = fd^2/D_v$. Simulations are performed with a wide range of frequencies and different values of h^* and D^*, assuming k^* to be the reciprocal of a linear sorption curve with a slope of 0.3. The results for a step change in the vapor concentration at the exposed surfaces from 0 to 1 are shown in Figure 10(a). For the limit of immediate equilibrium between vapor and cell wall water ($h^* = \infty$), the time evolution of the moisture content is equal to Equation (5). For slower sorption, i.e. with decreasing h^*, we see that the moisture content in the cell wall increases more slowly, as can be expected. Furthermore, for faster diffusion in the cell wall (higher value for D^*), the moisture content rises more quickly due to rapid redistribution of moisture in the cell wall.

The amplitude in moisture content in the cell wall as a function of the dimensionless frequency f^* is shown in Figure 10(b). For slow sorption, the amplitude is seen to decline at lower values of f^*. The dimensionless diffusion coefficient D^* has a minor influence on the frequency behavior. For high dimensionless frequencies f^*, the amplitude attains a constant slope of −1.4 on the logarithmic scale. This is

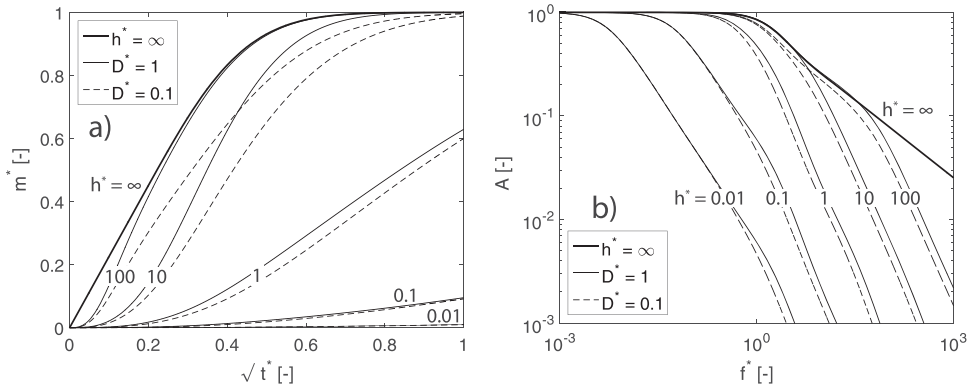

Figure 10. (a) Relative moisture content in a slab as a function of the square root of the scaled time t^* and (b) amplitude as a function of the dimensionless frequency f^* for different values of h^* and D^*.

considerably steeper than for the limit $h^* = \infty$, which yields a slope of −0.5. The experimental slopes are in between (−0.78 and −0.79); hence, sorption cannot account for the observed discrepancies in frequency behavior. More importantly, the value of the dimensionless mass transfer coefficient h^* is dependent on the sample size d (see Equation (19)). This was already noticed by Krabbenhoft and Damkilde (2004), who mentioned that the length of the sample influences the results in case vapor transfer is a faster process than sorption. It would therefore not be possible to simply scale results based on the sample size using the dimensionless frequency f^* in Equation (12). As already mentioned before, such a size effect is not apparent in the results found in this study and a previous study by the authors (Arends *et al.* 2017). The results for the differently sized cubes can be scaled onto a master curve based on their thickness alone, as shown in Figure 6. In case the introduced model would hold for our experiments, it would not be possible to scale all experiments onto one master curve as a function of f^*, but we would have different curves based on the parameter h^*, as shown in Figure 10(b). Hence, the influence of moisture sorption from the vapor phase to the cell wall cannot explain our experimental results and the observed discrepancy of our results with the frequency behavior predicted from the diffusion equation.

A similar effect is expected in case of a stationary boundary layer at the surfaces of the cube, which results in a resistance to moisture exchange. Scaling the equations yields a dimensionless mass transfer coefficient dependent on the sample size, similar to h^*. This contradicts the experimental findings of simple scaling of the frequency behavior. Mass transfer resistance, either internal in the porous structure or external on the macroscopic boundary, can therefore not account for the larger amplitude attenuation observed in the experiments compared to the diffusion equation.

Conclusions

The frequency behavior of moisture sorption and consequent expansion of oak cubes was studied experimentally. The amplitude in both moisture content and expansion as a function of frequency is shown to be scalable for the different sample sizes based on the length of the sides squared. Moreover, the frequency-dependent amplitude can be fitted to obtain the diffusion coefficients of the different samples, which are in agreement with values reported in literature. With these diffusion coefficients, a dimensionless frequency can be introduced based on the ratio of the transport timescale over the fluctuation timescale. By doing so, different regions can be distinguished in a scaled Bode plot.

Deviations in the frequency behavior are found between the prediction based on the diffusion equation and experiments. The slope of the amplitude at high frequencies differs, with a steeper amplitude decay found in the experiments. An additional effect thus attenuates both the moisture content and expansion amplitude at high frequencies. A parameter study using numerical modeling in COMSOL shows wood anisotropy for moisture transport and mechanical behavior cannot account for the observed differences in frequency behavior. Furthermore, an alternative moisture transport model with vapor diffusion in the cell cavities and bound water diffusion in the cell wall cannot explain the discrepancies either. The slope at high frequencies deviates significantly from experiments. Moreover, the alternative model contradicts scaling found from experiments based on sample size only, and can thus be disregarded.

Experiments in this study have been performed with all-sided exposure of the cubes to moisture. More information on transport in the different principal directions can be acquired with experiments sealing several surfaces to ensure one-dimensional transport. Additionally, expansion in other directions (radial, longitudinal) can be measured; it is, however, expected that the qualitative frequency behavior is similar, differing only in its magnitude. More information on moisture transport is expected from planned experiments with nuclear magnetic resonance.

Acknowledgements

The authors wish to thank J.H.J. Dalderop for his technical support. The work described in this paper has been carried out in the Darcy Center for porous media research and technology at Eindhoven University of Technology.

Disclosure statement

No potential conflict of interest was reported by the authors.

Funding

This work is part of the research program Science4Arts, financed by the Netherlands Organization for Scientific Research (NWO).

References

Arends, T., Pel, L. and Huinink, H.P. (2017) Hygromorphic response dynamics of oak: Towards accelerated material characterization. *Materials and Structures*, 50, 181.

Arends, T., Pel, L. and Smeulders, D.M.J. (2018) Moisture penetration in oak during sinusoidal humidity fluctuations studied by NMR. *Construction and Building Materials*, 166, 196–203.

Caré, S., Bornert, M., Bertrand, F. and Lenoir, N. (2012) Local moisture content and swelling strain in wood investigated by NMR and X-ray microtomography. In J.F. Silva Gomes and M.A.P. Vaz (eds.) *Proceedings of the 15th ICEM* (Porto, Portugal), 6pp.

Chomcharn, A. and Skaar, C. (1983) Dynamic sorption and hygroexpansion of wood wafers exposed to sinusoidally varying humidity. *Wood Science and Technology*, 17, 259–277.

Crank, J. (1975) *The Mathematics of Diffusion*, 2nd ed. (New York: Oxford University Press).

Cunningham, M. J. (1995) A model to explain "anomalous" moisture sorption in wood under step function driving forces. *Wood and Fiber Science*, 27, 265–277.

Dahlblom, O., Ormarsson, S. and Petersson, H. (1996) Simulation of wood deformation processes in drying and other types of environmental loading. *Annals of Forest Science*, 53, 857–866.

Derome, D., Rafsanjani, A., Patera, A., Guyer, R. and Carmeliet J. (2012) Hygromorphic behaviour of cellular material: hysteretic swelling and shrinkage of wood probed by phase contrast X-ray tomography. *Philosophical Magazine*, 92, 1–21.

Dvinskikh, S.V., Henriksson, M., Mendicinod, A.L., Fortino, S. and Toratti, T. (2011) NMR imaging study and multi-Fickian numerical simulation of moisture transfer in Norway spruce samples. *Engineering Structures*, 33, 3079–3086.

Eitelberger, J., Hofstetter, K. and Dvinskikh, S.V. (2011) A multi-scale approach for simulation of transient moisture transport processes in wood below the fiber saturation point. *Composites Science and Technology*, 71, 1727–1738.

Forest Products Laboratory (2010) *Wood Handbook – Wood as an Engineering Material* (Madison, WI: United States Department of Agriculture).

Franklin, G.F., Powell, J.D. and Emami-Naeini, A. (1994) *Feedback Control of Dynamic Systems*, 3rd ed. (Reading, MA: Addison-Wesley).

Gamstedt, E.K., Bader, T.K. and de Borst, K. (2013) Mixed numerical-experimental methods in wood micromechanics. *Wood Science and Technology*, 47, 183–202.

Gauvin, C., Jullien, D., Dupré, J.-C. and Gril, J. (2014) Image correlation to evaluate the influence of hygrothermal loading on wood. *Strain*, 50, 428–435.

Jakiela, S., Bratasz, L. and Kozlowski, R. (2008) Numerical modelling of moisture movement and related stress field in lime wood subjected to changing climate conditions. *Wood Science and Technology*, 42, 21–37.

Joffre, T., Isaksson, P., Dumont, P.J.J., Rollanddu Roscoat, S., Sticko, S., Orgéas, L. and Gamstedt, E.K. (2016) A method to measure moisture induced swelling properties of a single wood cell. *Experimental Mechanics*, 56, 723–733.

Krabbenhoft, K. and Damkilde, L. (2004) A model for non-Fickian moisture transfer in wood. *Materials and Structures*, 37, 615–622.

Larsen, F. and Ormarsson, S. (2013) Numerical and experimental study of moisture-induced stress and strain field developments in timber logs. *Wood Science and Technology*, 47, 837–852.

Ma, E., Zhao, G. and Cao, J. (2005) Hygroexpansion of wood during moisture adsorption and desorption processes. *Forestry Studies in China*, 7(2), 43–46.

Mazzanti, P., Colmars, J., Gril, J., Hunt, D. and Uzielli, L. (2014) A hygro-mechanical analysis of poplar wood along the tangential direction by restrained swelling test. *Wood Science and Technology*, 48, 673–687.

Mecklenburg, M.F. and Tumosa, C.S. (1996) The relationship of externally applied stresses to environmentally induced stresses. In H. Saadatmanesh and M.R. Ehsani (eds.) *Fiber Composites in Infrastructure* (Tucson, Arizona), pp. 956–971.

Murata, K. and Masuda, M. (2006) Microscopic observation of transverse swelling of latewood tracheid: effect if macroscopic/mesoscopic structure. *Journal of Wood Science*, 52, 283–289.

Ormarsson, S., Dahlblom, O. and Petersson, H. (1998) A numerical study of the shape stability of sawn timber subjected to moisture variation. Part 1: Theory. *Wood Science and Technology*, 32, 325–334.

Saft, S. and Kaliske, M. (2013) A hybrid interface-element for the simulation of moisture induced cracks in wood. *Engineering Fracture Mechanics*, 102, 32–50.

Schellen, H.L. (2002) *Heating Monumental Churches: Indoor Climate and Preservation of Cultural Heritage* Thesis (PhD). Eindhoven University of Technology.

Senni, L., Caponero, M., Casieri, C., Felli, F. and De Luca, F. (2010) Moisture content and strain relation in wood by Bragg grating sensor and unilateral NMR. *Wood Science and Technology*, 27, 409–420.

Siau, J. F. (1984) *Transport Processes in Wood* (Berlin: Springer).

Skaar, C. (1988) *Wood-water Relations* (Berlin: Springer-Verlag).

Strauss, W. A. (2008) *Partial Differential Equations: An Introduction* 2nd ed. (Hoboken, NJ: John Wiley & Sons).

Svensson, S. and Toratti, T. (2002) Mechanical response of wood perpendicular to grain when subjected to changes of humidity. *Wood Science and Technology*, 36, 145–156.

Talbot, A. and Kitchener, J. A. (1956) Diffusion (or conduction) along a slightly tapering tube, and its application to the determination of diffusion coefficients. *British Journal of Applied Physics*, 7, 96–97.

van Schijndel, A. W. M., Schellen, H. L. and Timmermans, W. J. (2010) Simulation of the climate system performance of a museum in case of failure events. *Energy and Buildings*, 42, 1790–1796.

Wadsö, L. (1994a) Describing non-Fickian water-vapour sorption in wood. *Journal of Materials Science*, 29, 2367–2373.

Wadsö, L. (1994b) Unsteady-state water vapour adsorption in wood: An experimental study. *Wood and Fiber Science*, 6(1), 36–45.

Yang, T. and Ma, E. (2014) Dynamic sorption and hygroexpansion of wood subjected to cyclic relative humidity changes. II. Effect of temperature. *BioResources*, 10, 1675–1685.

Zhou, Y., Fushitani, M., Kubo, T. and Ozawa, M. (1999) Bending creep behavior of wood under cyclic moisture changes. *Journal of Wood Science*, 45, 113–119.